Heliyon 7 (2021) e07819

Contents lists available at ScienceDirect

Heliyon

journal homepage: www.cell.com/heliyon

Research article

The comparison of the properties of nanocellulose isolated from colonial and solitary marine tunicates

Naphatson Chanthathamrongsiri [a,b], Arpa Petchsomrit [a], Nattawut Leelakanok [a], Nisa Siranonthana [c], Thanchanok Sirirak [a,b,*]

[a] Faculty of Pharmaceutical Sciences, Burapha University, Chonburi, Thailand
[b] The Research Unit in Synthetic Compounds and Synthetic Analogues from Natural Products for Drug Discovery, Burapha University, Chonburi, Thailand
[c] Institute of Marine Science, Burapha University, Chonburi, Thailand

ARTICLE INFO

Keywords:
Tunicate composite
Nanocellulose
Biomaterials
Natural product chemistry
Material characterization

ABSTRACT

This is the first comparative of tunicate cellulose nanocrystalline (t-CNC) from colonial and solitary tunicates. The t-CNC from the colonial tunicate *Eudistoma* sp. (CL1) was compared with solitary tunicates *Polycarpa reniformis* (CL2) and *Phallusia nigra* (CL3). Tunicate samples were extracted by methanol. Residues from the methanol extraction were then subjected to further cellulose purification using pre-hydrolysis, kraft-cooking, bleaching, and sulfuric acid hydrolysis to yield t-CNC. The solitary tunicates yielded higher microfibril contents after the bleaching step but obtained similar t-CNC content to the colonial one after acid hydrolysis. The isolated t-CNC were characterized using Fourier transform infrared spectroscopy, X-ray diffraction, thermalgravimetric analysis, and transmission electron microscopy. Both colonial and solitary tunicates yielded cellulose type I. The pure cellulose type I was successfully isolated from solitary tunicates whereas high inorganic impurities were observed in colonial tunicates. The isolate t-CNC showed high aspect ratios. The solitary and colonial tunicates provided t-CNC with crystallinity indexes over 97% and 35%, respectively. The crystalline size of t-CNCs ranged from 55-124 Å. The thermal stability of all isolated t-CNC was slightly decreased due to the sulfate functional groups gained after acid hydrolysis. We concluded that solitary tunicates were better than colonial tunicates as a source of t-CNC preparation.

1. Introduction

Cellulose is the most abundant biopolymer on earth and ubiquitously found in plants, marine animals, algae, and bacteria. Because of its abundance, renewability, sustainability, and biocompatibility, cellulose has recently been highlighted for further development, thus increasing demand by customers and industry [1]. The goal for the development of the cellulose-based product is to increase crystallinity and mechanical properties. Searching for new sources of cellulose is one of the modalities used for improving the quality of cellulose. Currently, plants are the only source of commercially available cellulose. Bacteria are the other sources that provide higher quality cellulose and the bacterial cultivation process is more eco-friendly than plant-based cellulose [2]. However, the production of both plant-based and bacterial-based cellulose is land-based. Marine aquaculture for cellulose from tunicates (subphylum Tunicata, class Ascidiacea), which are the only animals that can synthesize cellulose, is an alternative that can decrease land requirements, be eco-friendly, and help in carbon sequestration back to the ocean floor [3, 4].

Besides the advantage of the mode of tunicate cultivation, tunicate cellulose is high in quality. Tunicate cellulose forms complexes with proteins to make their external protective structure or tunic. The cellulose nanofibrils are bundled in a multiple-layered texture parallel to the tunic surface. The shape and dimensions of nanofibrils vary depending on species [5]; although the cellulose properties are expected to be comparable between species and to possibly have a slight difference in microfibril formation [6]. Tunicate nanofibrils typically have lengths ranging from 100 nm to several micrometers (2 μm), widths ranging from 10-30 nm, and aspect ratios ranging from 70-100 [7]. The highly reactive surface area of tunicate cellulose makes it an excellent material to cross-link with other devices and biomedical applications [8, 9]. The tunicate cellulose is highly crystalline (85–100%) and contains I_β crystal structure [10]. The quality of tunicate cellulose is superior to plant-based cellulose in terms of molecular weight, mechanical properties, water

* Corresponding author.
E-mail address: Thanchanoks@go.buu.ac.th (T. Sirirak).

https://doi.org/10.1016/j.heliyon.2021.e07819
Received 12 January 2021; Received in revised form 11 July 2021; Accepted 13 August 2021

holding capacity, permeability, and thermal stability [11]. Besides, the crystallinity index (CI) of tunicate cellulose is comparable to the CI of algal cellulose and higher than plant-based cellulose and bacterial cellulose [5].

Because of the variation of tunicate cellulose in different tunicate species, studies on the properties of tunicate cellulose from different species are required. Based on body structure and functional organization, tunicates are classified into colonial and solitary types. Solitary tunicates live separately inside their tunic, whereas colonial tunicates are physically connected with a common tunic that they budded off [12, 13]. Most of the research in tunicate cellulose focused on solitary tunicates including *Ciona intestinalis* [5, 14, 15, 16], *Ascidia* sp. [5, 15], *Halocynthia roretzi* [5, 15, 17], *Styela plicata* [5, 15], *Styela clava* [14, 18], *Halocynthia papillosa* [19, 20], and *Metandrocarpa uedai* [6]. However, the study on cellulose from colonial tunicates is limited. To the best of our knowledge, this is the first study that compares cellulose characteristics from colony tunicates, *Eudistoma* sp., to cellulose from solitary tunicates, *Polycarpa reniformis,* and *Phallusia nigra*. The result from this study can be used as a pilot in utilizing cellulose from other colonial tunicates, especially the pestilence and invasive species such as *Didemnum vexillum* [21].

2. Experimental

2.1. Materials

The colonial tunicate *Eudistoma* sp. (CL1) was collected by hand from a floating fish cage in the Sea Farming Demonstration Unit, Chanthaburi in 2017. The solitary tunicates were collected from Srichang Islands, Chonburi, Thailand. *Polycarpa reniformis* (CL2) was collected by SCUBA diving at 15 m depth in 2017, while *Phallusia nigra* (CL3) [22, 23] was collected by hand from a floating cage in 2016. Freeze-dried tunicates were extracted exhaustively with methanol (1:20) approximately 3–4 times to remove all bioactive compounds. The residues were dried and stored at -20 °C until used. All reagents used, including sulfuric acid (H_2SO_4: RCI Labscan, Bangkok, Thailand), acetone ($(CH_3)_2CO$, ChemLab, Belgium), sodium hydroxide (NaOH: Loba Chemie, India), sodium sulfide (Na_2S, Loba Chemie, India), and sodium hypochloride (NaClO, Loba Chemie, India), were analytical grade.

2.2. Extraction of nanocellulose

The freeze-dried tunicate residues were extracted by pre-hydrolysis, kraft-cooking, bleaching (to obtain tunicate cellulose microfibril (t-CMF) [5]), and acid hydrolysis (to obtain tunicate nanocrystal (t-CNC) [18]). Briefly, the dried residue of each tunicate was pre-hydrolyzed by refluxing with 1% aq H_2SO_4 for 2 h. The neutralized residue with water:acetone (1:1) was further refluxed with 9%/3% NaOH/Na_2S for 2 h. The sample was washed with water:acetone until a pH of approximately 7 was reached. The freeze-dried sample was bleached 2–3 times by boiling with 3% NaClO at 75 °C for 1 h to yield t-CMF. The t-CMF was homogenized with water and was treated with 60% sulfuric acid at 60 °C for 60 min. The sample was filtered and neutralized with water:acetone to obtain t-CNC. The sample was freeze-dried. Solid yields were calculated by comparing the weight of lyophilized sample weight with the dried tunic weight.

2.3. Characterizations

The functional groups were determined using an ATR-FTIR Nicolet 6700 FT-IR Spectrometer (Thermo Fischer Scientific, USA) and recorded with OMNIC FT-IR software. The surface morphology of isolated cellulose was observed using a LEO1450VP Scanning Electron Microscope (Zeiss, Germany) at 15 kV. The sample was coated with gold (Au) before determination. The ash content was determined by heating the sample at 550 °C for 6 h. The value was calculated based on residue after the gravimetric determination. The TEM image was obtained from a Philips Tecni20 (Thermo Fischer Scientific, USA). The t-CNC 0.1% w/v was suspended in water and sonicated for 10 min and then was deposited onto the TEM grid. The sample was stained with 2% phosphotungstic acid. The diameter width and length of t-CNC were measured using a two-point analysis, which calibrated length with the provided scale on the TEM image (ImageJ 1.525v software, National Institute of Mental Health, USA). The length-width aspect ratios were calculated from 50 measurements [24]. The zeta potential was determined by dynamic light scattering using a Zetasizer Nano ZS (Malvern Instrument Ltd., Worcestershire, UK) at 25 °C. The crystallinity was carried out using Aeris XRD diffractometer (Malvern Panalytical, Netherland) with monochromatic CuKα radiation (λ = 1.54060 Å, 40.0 kV, 40.0 mA, $10° < 2\theta < 50°$, 0.043466° at 2 s/step). The crystallinity index was calculated using the following Eq. (1) [5, 25]:

$$Crystallinity\ index = \left(\frac{I_{200} - I_{am}}{I_{200}}\right) \times 100 \quad (1)$$

where I_{200} is the intensity of the (200) lattice plane at $2\theta = 22.8°$, and I_{am} is the intensity from the amorphous phase, which approximately $2\theta = 18°$. The crystalline size was calculated according to the Scherrer equation [5, 26] (HighScore 5.0 software, Malvern Panalytical, Netherland). The thermal decomposition profiles were investigated by PerkinElmer TGA4000 (PerkinElmer, USA). The heating was from 50 °C to 800 °C, increasing gradually at the rate of 10 °C/min, and was carried out under an inert nitrogen atmosphere flowing at 20 mL/min.

3. Results and discussions

Cellulose composition was carried out on a colonial tunicate *Eudistoma* sp. (CL1) and two solitary tunicates including *Polycarpa reniformis* (CL2) and *Phallusia nigra* (CL3) (Figure 1a-c). The three samples were obtained as debris after chemical extraction (Figure 1d-f). The freeze-dried debris was pre-hydrolyzed with acid and later subjected to alkaline treatment in the kraft-cooking process to yield bleached tunic or cellulose microfibrils (t-CMF). A large amount of weight was lost in these steps for all samples (Table 1) due to the removal of lipid, ash, and protein content [5]. Higher weight loss was observed in the colonial sample, indicating that the colonial tunicate *Eudistoma* sp. was composed of higher protein content than the other two solitary tunicates (Figure 1g-i). After acid hydrolysis, the t-CMF mass of solitary tunicates (CL2 and CL3) decreased more than the colonial tunicate, suggesting microfibrils in solitary tunicates composed of an amorphous domain more than in the colonial species.

The structure of cellulose during the isolation process was carried out by FTIR spectroscopy (Figure 2). The tunic of tunicates was constructed by cellulose-protein fibril which was cemented with sulfated polysaccharides and lipids [15]. The sulfated polysaccharide structure was verified with FTIR which exhibited broadband of sulfate ester at 1220-1260 cm^{-1} and the signal of S=O at 1240 cm^{-1}. The intense peak at 1,610 cm^{-1} and 1,540 cm^{-1} was assigned as amide linkage [5, 27]. In this study, the signals of stretching vibration of charged carboxylated at 1628 cm^{-1} and antisymmetric of SO_3^- stretching mode in a range of 1200–1450 cm^{-1} were observed in untreated tunic. The signals were reduced after NaOH treatment and the bleaching process (Figure 2b). The bleached cellulose and isolated t-CNC showed similar FTIR spectra meaning that the chemical structure of t-CNC, which was the type I cellulose, was similar to their bleached cellulose. The spectrum of t-CNC showed a broad peak at 3335 cm^{-1}, indicating O–H stretching of hydrogen bonding between functional groups, while absorbed water showed O–H bending vibration at a wavenumber of 1634 cm^{-1}. The absorbances at around 2867-2967 cm^{-1} and 1370-1428 cm^{-1} indicated C–H stretching and C–H bending of the pyranose ring, respectively. Glycosidic linkages were determined at the “anomeric region”, ranging from 1200-950 cm^{-1}, and presented characteristic bands of C–O and C–C groups. The peak at 1054 cm^{-1} was assigned as the C–O–C group of

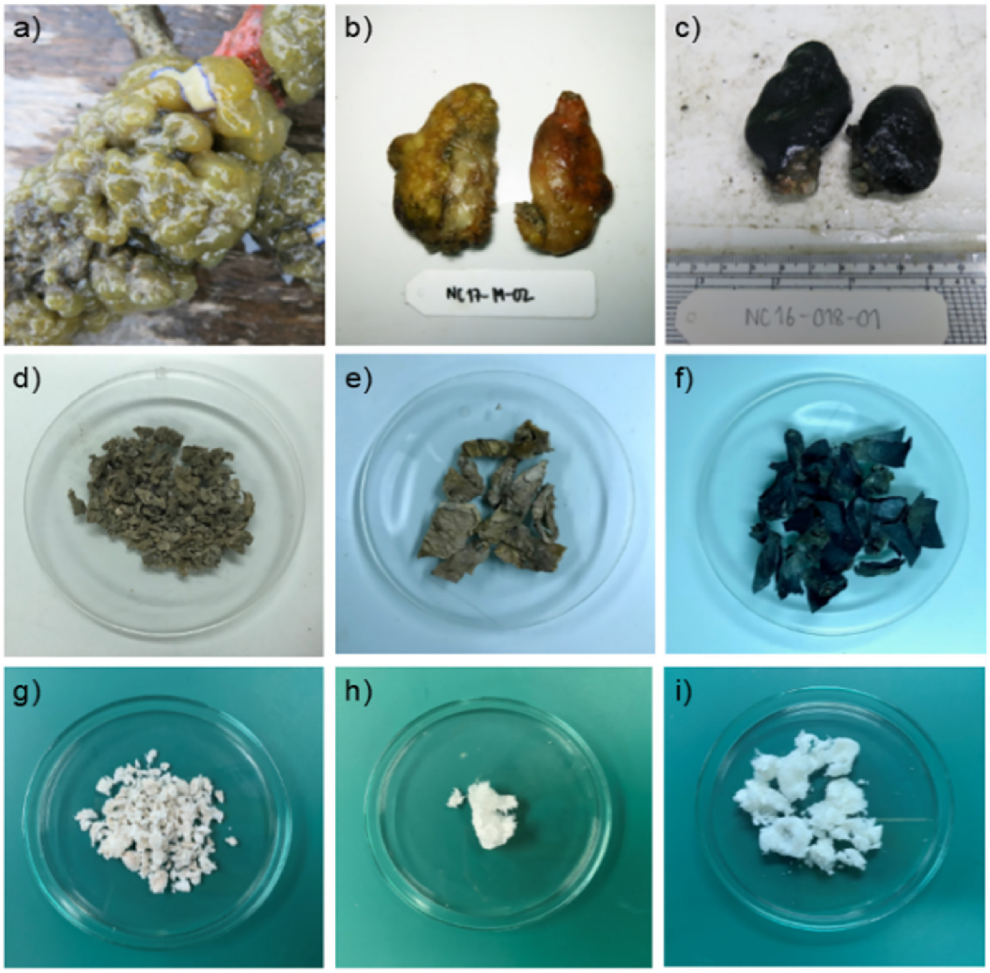

Figure 1. Appearance on the surface (a–c), freeze-dried debris for cellulose extraction (d–f), and 0.2 g purified cellulose nanocrystal (g–i) of tunicates *Eudistoma* sp., *Polycarpa reniformis*, and *Phallusia nigra*, respectively.

Table 1. Mass yield of the overall process.

Tunicate species	Solid yield (%)			
	Pre-hydrolysis	Kraft cooking	Bleaching	H_2SO_4 hydrolysis
Eudistoma sp.	20.46	5.48	4.51	2.19
Polycarpa reniformis	33.69	24.82	23.42	1.32
Phallusia nigra	35.96	22.31	21.38	5.28

pyranose rings [28]. All three isolated nanocellulose samples were assigned as β-linkage with peaks at 898 cm^{-1} [29]. Absorption peaks at 3270 cm^{-1} and 710 cm^{-1} indicated that all three isolated celluloses were in cellulose I_β form [30, 31]. The absence of signals at 1240 cm^{-1}, 1267 cm^{-1}, 1460 cm^{-1}, and 1570 cm^{-1}; 1640-1655 cm^{-1}; and 1540 cm^{-1}, respectively, revealed that the isolated cellulose nanocrystals were free from lignin and protein [32, 33].

After the purification process, the inorganic impurity components were supposed to be removed. However, in this study, the t-CNC CL1 had a high ash level, which represented the number of inorganic impurities, of 50.97%, while CL2 and CL3 had a low ash level of 2.05% and 0.79%, respectively. Sea salts and inorganic compounds were major components in tunicate samples. Different salinity in the different seas could explain the variances in inorganic matters [34]. The tunicates are non-selective filter feeders that accumulate various inorganic compounds in their organs and tunic. The high ash content was observed in colonial tunicates CL1 which could be owing to the looser and softer tunic structure that allows seawater to penetrate and retain in the tissue [15].

SEM imaging was used to determine the morphological structure of the bleached tunic before acid hydrolysis, and TEM imaging was used to determine the morphological structure of t-CNC. The SEM image of bleached tunics (Figure 3) shows that the cellulose was aggregated in the form of microfibrils and the chains weaved together like a tight net. The diameter size in a range of 52–90 nm for CL1-3. The microfibrils of CL1 and CL2 were more bundled than CL3. This was inconsistent with the report from Zhao and Li [5], whose results show that microfibrils of hard and thick tunics are more bundled than soft tunics. In this study, cellulose microfibrils from the thick tunic of *Phallusia nigra* (CL3) showed less bundled than the soft tunic, *Eudistoma* sp. The result was probably because *P. nigra* produces sulfuric acid, SO_4^{2-}, and Cl^- as major ions [35] and some sulfate functional groups might be introduced into the surface of microfibrils. Microfibril bundles aggregate less due to the surface

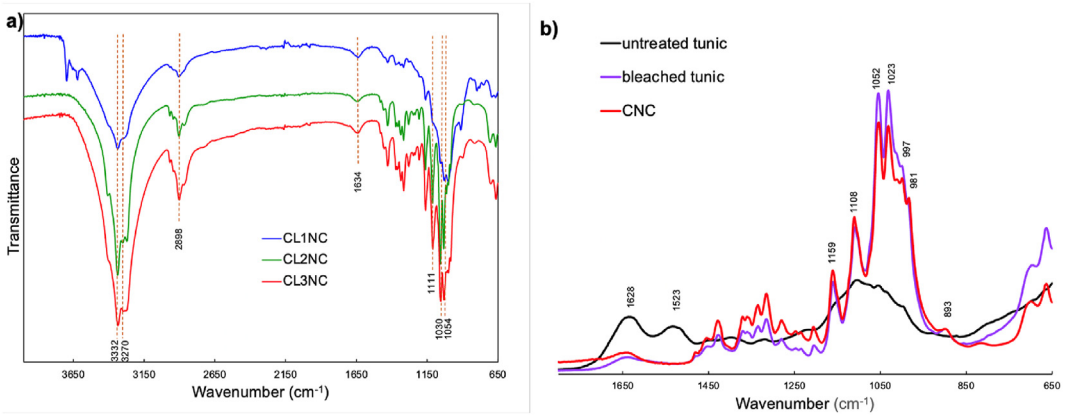

Figure 2. a) FTIR spectra of nanocellulose isolated from *Eudistoma* sp. (CL1NC), *Polycarpa reniformis* (CL2NC), and *Phallusia nigra* (CL3NC); b) FTIR spectra changes of *Phallusia nigra* during isolation process. Similar FTIR spectra change trends were observed for all of the other samples.

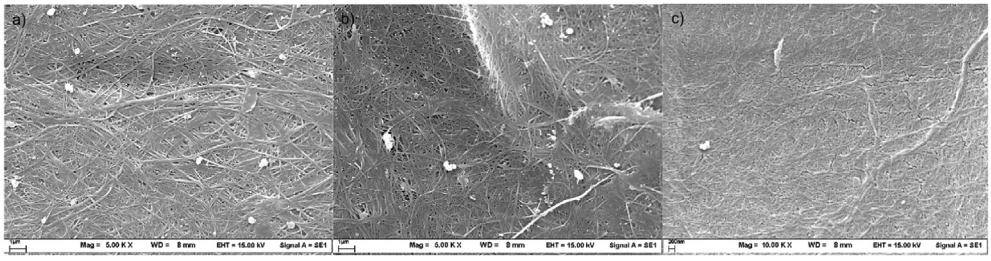

Figure 3. SEM images of bleached tunic from *Eudistoma* sp. (a), *Polycarpa reniformis* (b), and *Phallusia nigra* (c).

negative charge, which might come from the incorporated sulfate group, on their surfaces that leads to internal electrostatic repulsion [36].

The shape and dimension of isolated t-CNC were investigated using transmission electron microscopy (TEM) (Figure 4). The TEM images of t-CNC showed a well dispersed and less tendency to aggregate at a concentration of 0.1% w/v. The rod-like structure was observed with some kink due to mechanical damage [37]. The dimensions of isolated t-CNC are in the same range as typical t-CNC [10]. The width of CL2 (24.6 ± 1.12 nm) was larger than CL1 (14.4 ± 0.9 nm) and CL3 (12.2 ± 0.9 nm) and the length of CL2 (1.95 ± 1.12 μm) was also longer than CL1 (1.08 ± 0.69 μm) and CL3 (0.67 ± 0.20 μm). The aspect ratios were calculated as the length divided by the width for individual nanocellulose. All isolated t-CNC showed high aspect ratios, ranging from 65-86. The aspect ratio distribution is shown in Figure 5. According to these findings, the size and aspect ratio of tunicate nanocellulose varied by species rather than by the morphological type shown in a prior study [18].

The t-CNC were well dispersed in water (Figure 4) due to the sulfate groups obtaining during acid hydrolysis [38]. The sulfate ester groups influencing the surface charge of t-CNC suspensions with the zeta potential of -27.7 ± 0.79 mV, -31.8 ± 1.01 mV, and -38.9 ± 2.72 mV for CL1-CL3, respectively. The suspension with a zeta potential value that is not in the range of −30 mV to +30 mV is considered a stable colloid system [39]. From these results, the nanosuspension of CL2 and CL3 showed a larger negative zeta potential value with more negative than -30 mV. Therefore, the nanosuspensions systems of the sample CL2 and CL3 were more stable than that of the CL1. These results corresponded with previous reports showing that the higher surface charged of t-CNC had sufficient electrostatic repulsion, resulting in better aqueous dispersion [36, 39].

The crystalline characteristics of bleached specimens and t-CNC were carried out using powder X-ray diffractometry. The diffractograms of all bleached samples showed native cellulose type I peaks at 15.1°, 16.9°, and 23.2° (Figure 6), which were correlated with (110), (1$\bar{1}$0), and (200) refractometry, respectively [5, 40]. In all the bleached samples, there was no evidence of cellulose type II at 12° (110), 20° (1$\bar{1}$0), and 22° (200) [41]. The presence of cellulose type I in the bleached samples indicating that methanol treatment of the samples before cellulose extraction did not affect to cellulose allomorph conversion. Additional crystalline peaks were only found in the bleached CL1 sample, which could be attributed to mineral seawater trapping during the drying method. After sulfuric acid hydrolysis, the t-CNC from CL2 and CL3 still showed the typical reflection of cellulose I indicating that the crystal integrity had been maintained with crystalline indexes of 99.1%, and 95.5%, respectively. The main peaks of the t-CNC CL1 showed lower intensity and slightly shifted to lower 2θ. After acid hydrolysis, the peaks at ~12° and ~20° occurred, indicating the presence of cellulose type II that could be

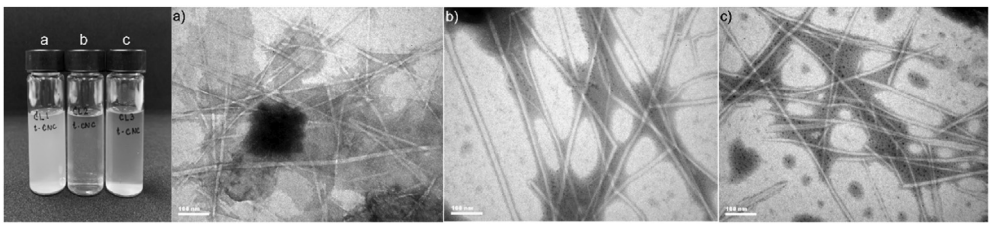

Figure 4. 2%w/v suspension and TEM images of 0.1%w/v tunicate nanocrystal from *Eudistoma* sp. (a), *Polycarpa reniformis* (b), and *Phallusia nigra* (c).

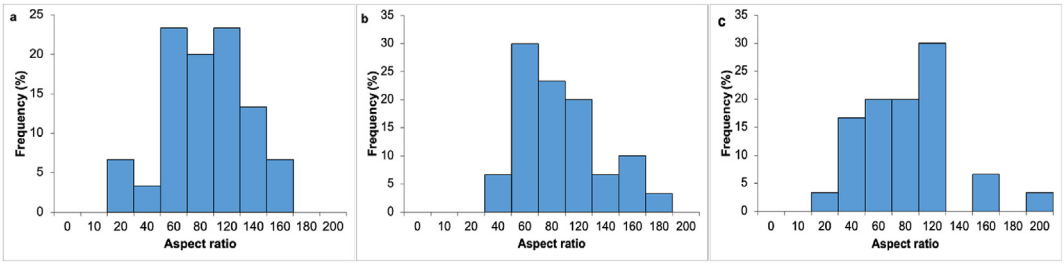

Figure 5. The length-width aspect ratio distribution of nanocellulose isolated from *Eudistoma* sp. (a), *Polycarpa reniformis* (b), and *Phallusia nigra* (c).

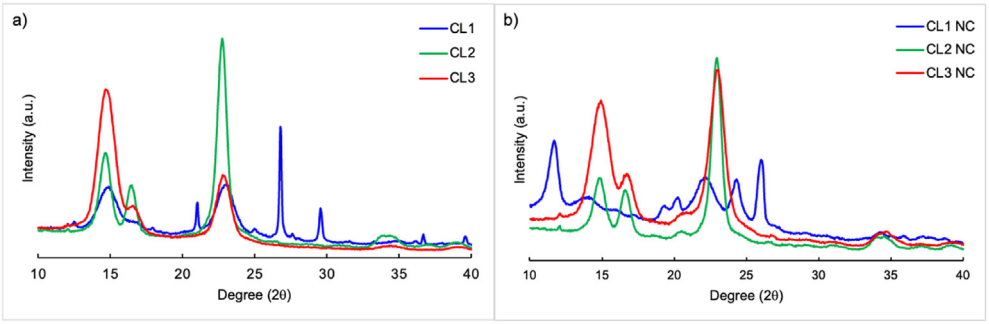

Figure 6. The X-ray diffractogram of the bleached tunic (a) and cellulose nanocrystals (b) isolated from tunicates *Eudistoma* sp. (CL1), *Polycarpa reniformis* (CL2), and *Phallusia nigra* (CL3).

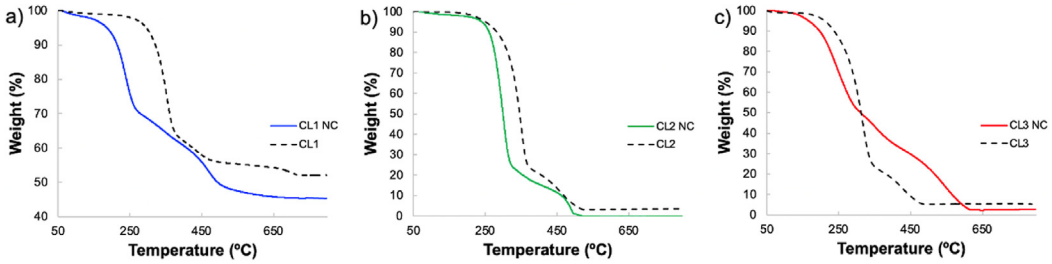

Figure 7. Thermogravimetric curve of the bleached tunic (CL1-3) and nanocellulose (CL1-3 NC) from *Eudistoma* sp. (a), *Polycarpa reniformis* (b), and *Phallusia nigra* (c), respectively.

converted from cellulose I under the acidic condition [42]. The cellulose I crystallinity index of CL1 was decreased from 89.6% to 35.7% after acid hydrolysis suggesting that the cellulose crystals were dissolved and converted to an amorphous form with a broad signal between 17° and 28° (Figure 6b). The calculated crystal size of (200) diffraction of CL1-3 t-CNC was 55 Å, 124 Å, and 74 Å, respectively. The crystal size of t-CNC from the soft colonial tunicate was smaller than that from solitary tunicates. Although no t-CNC from colonial tunicates has been reported, the stiffness of tunic from solitary tunicates revealed a similar crystal size trend. Soft tunics, *Ciona intestinalis* and *Ascidia* sp., had smaller crystal sizes of 60.6 Å and 60.2 Å, whereas thicker tunics, *Halocynthia roretzi,* and *Styela plicata*, had the crystal sizes of 73.2 Å and 81.0 Å, respectively [5]. A similar pattern was observed in the analysis of nanocellulose from soft tunics of vase tunicates and thick tunics of club tunicates with sizes of 94.0 Å and 112.3 Å, respectively [14].

The thermal decomposition profiles of t-CNC using TGA were compared to the bleached sample and are shown in Figure 7. All t-CNC showed small weight loss (0.7–1.8%) at a temperature between 60 °C and 80 °C due to the evaporation of adsorbed water. The TGA profiles of t-CNC showed that the thermostability of t-CNC was lower than their bleached sample. The preparation of t-CNC using sulfuric acid hydrolysis are well known to introduce sulfate group into cellulose surface and decrease t-CNC thermostability [43]. The onset degradation (T_0) of t-CNC was increased in the following order CL3> CL1>CL2 (187 °C, 203 °C, and 265 °C, respectively). The TGA profiles of t-CNC showed similar profiles with two distinct pyrolysis processes. All TGA of t-CNC had decomposition temperatures (T_{max} 237–294 °C) lower than the temperature of their bleached samples (T_{max} 324–352 °C). The lower degradation temperature at approximately 200 °C corresponded to the degradation of the accessible, highly sulfated, and amorphous region, whereas the higher degradation temperature at approximately 400 °C related to the unsulfated crystal interior. The t-CNC CL1 had lower thermal stability than the others when compared to their bleached sample. The lower thermal deterioration could be attributed to an increase in amorphous content [36].

4. Conclusions

This study showed that both colonial tunicates, *Eudistoma* sp., and solitary tunicates, *Polycarpa reniformis* and *Phallusia nigra*, comprised of native cellulose type I. The cellulose nanocrystal (t-CNC) was prepared by pre-hydrolysis, kraft-cooking, bleaching, and acid hydrolysis sequences. Solitary tunicates yielded pure nanocellulose type I, whereas colonial tunicates yielded t-CNC with significant inorganic impurities. The soft tunic of colony tunicates, as well as the intact organ-to-tunic interface, allows more sea salts and inorganic impurities to be retained than in solitary tunicates. The size and aspect ratios of isolated t-CNC vary,

depending on tunicate species. The t-CNC from solitary tunicates showed better mechanical properties than colonial tunicates with a higher crystallinity index and crystalline size. All isolated t-CNC nanosuspension is stable with significant negative charges repulsion of sulfate groups which decreased the thermal stability of t-CNC. However, both colonial and solitary tunicates are the source of nanocellulose with high crystalline and aspect ratios better than nanocellulose from wood.

Declarations

Author contribution statement

Naphatson Chanthathamrongsiri: Conceived and designed the experiments; Contributed reagents, materials, analysis tools or data.

Arpa Petchsomrit: Performed the experiments; Analyzed and interpreted the data; Contributed reagents, materials, analysis tools or data; Wrote the paper.

Nattawut Leelakanok: Contributed reagents, materials, analysis tools or data; Wrote the paper.

Nisa Siranonthana: Performed the experiments; Contributed reagents, materials, analysis tools or data.

Thanchanok Sirirak: Conceived and designed the experiments; Performed the experiments; Analyzed and interpreted the data; Contributed reagents, materials, analysis tools or data; Wrote the paper.

Funding statement

This work was supported by Faculty of Pharmaceutical Sciences, Burapha University (grant no. 2/2560) and The Research Unit in Synthetic Compounds and Synthetic Analogues from Natural Product for Drug Discovery (RSND).

Data availability statement

Data included in article/supplementary material/referenced in article.

Declaration of interests statement

The authors declare no conflict of interest.

Additional information

No additional information is available for this paper.

Acknowledgements

We would like to thank Dr. Sumaitt Putchakarn from the Marine Science Institute, Burapha University for tunicate identification, and Mr. Thakorn Kakhaikitthawat, Kung Krabaen Bay Royal Development Study Center, Chanthaburi for their kind support.

References

[1] K. Dhali, et al., A review of nanocellulose as a new material towards environmental sustainability, Sci. Total Environ. 775 (2021) 145871.
[2] S.M. Choi, E.J. Shin, The nanofication and functionalization of bacterial cellulose and its applications, Nanomaterials 10 (3) (2020) 406.
[3] M.J.J. Theuerkauf SJ, T.J. Waters, L.C. Wickliffe, H.K. Alleway, R.C. Jones, A global spatial analysis reveals where marine aquaculture can benefit nature and people, PloS One 14 (10) (2019) e0222282.
[4] R.R. Gentry, et al., Exploring the potential for marine aquaculture to contribute to ecosystem services, Rev. Aquacult. 12 (2) (2020) 499–512.
[5] Y. Zhao, J. Li, Excellent chemical and material cellulose from tunicates: diversity in cellulose production yield and chemical and morphological structures from different tunicate species, Cellulose 21 (5) (2014) 3427–3441.
[6] S. Kimura, T. Itoh, New cellulose synthesizing complexes (terminal complexes) involved in animal cellulose biosynthesis in the tunicateMetandrocarpa uedai, Protoplasma 194 (3) (1996) 151–163.
[7] H. Seddiqi, et al., Cellulose and its derivatives: towards biomedical applications, Cellulose 28 (4) (2021) 1893–1931.
[8] A. Parry, Nanocellulose and its composites for biomedical applications, Curr. Med. Chem. 23 (2016).
[9] M. Jorfi, E.J. Foster, Recent advances in nanocellulose for biomedical applications, J. Appl. Polym. Sci. 132 (14) (2015).
[10] R.J. Moon, et al., Cellulose nanomaterials review: structure, properties and nanocomposites, Chem. Soc. Rev. 40 (7) (2011) 3941–3994.
[11] Y. Zhao, C. Moser, G. Henriksson, Transparent composites made from tunicate cellulose membranes and environmentally friendly polyester, ChemSusChem 11 (10) (2018) 1728–1735.
[12] S.H. Kassmer, S. Nourizadeh, A.W. De Tomaso, Cellular and molecular mechanisms of regeneration in colonial and solitary Ascidians, Dev. Biol. 448 (2) (2019) 271–278.
[13] J.B.C. Jackson, Competition on marine hard substrata: the adaptive significance of solitary and colonial strategies, Am. Nat. 111 (980) (1977) 743–767.
[14] M.J. Dunlop, B. Acharya, R. Bissessur, Isolation of nanocrystalline cellulose from tunicates, J. Environ. Chem. Eng. 6 (4) (2018) 4408–4412.
[15] Y. Zhao, J. Li, Ascidian bioresources: common and variant chemical compositions and exploitation strategy – examples of Halocynthia roretzi, Styela plicata, Ascidia sp. and Ciona intestinalis, Z. Naturforsch. C Biosci. 71 (5-6) (2016) 165–180.
[16] Y. Zhao, et al., Cellulose nanofibers from softwood, hardwood, and tunicate: preparation–structure–film performance interrelation, ACS Appl. Mater. Interfaces 9 (15) (2017) 13508–13519.
[17] S.M. Moon, et al., High crystallinity of tunicate cellulose nanofibers for high-performance engineering films, Carbohydr. Polym. 254 (2021) 117470.
[18] I.A. Sacui, et al., Comparison of the properties of cellulose nanocrystals and cellulose nanofibrils isolated from bacteria, tunicate, and wood processed using acid, enzymatic, mechanical, and oxidative methods, ACS Appl. Mater. Interfaces 6 (9) (2014) 6127–6138.
[19] W. Helbert, et al., Molecular imaging ofHalocynthia papillosaCellulose, J. Struct. Biol. 124 (1) (1998) 42–50.
[20] S. Iwamoto, et al., Elastic modulus of single cellulose microfibrils from tunicate measured by atomic force microscopy, Biomacromolecules 10 (9) (2009) 2571–2576.
[21] L.-M. Herborg, P. O'Hara, T.W. Therriault, Forecasting the potential distribution of the invasive tunicate Didemnum vexillum, J. Appl. Ecol. 46 (1) (2009) 64–72.
[22] L.E. Vandepas, et al., Biogeography of Phallusia nigra: is it really black and white? Biol. Bull. 228 (1) (2015) 52–64.
[23] M. Çinar, et al., New records of alien species on the Levantine coast of Turkey, Aquat. Invasions 1 (2006) 84–90.
[24] M.J. Dunlop, B. Acharya, R. Bissessur, Study of plant and tunicate based nanocrystalline cellulose in hybrid polymeric nanocomposites, Cellulose 27 (1) (2020) 249–261.
[25] L. Segal, et al., An empirical method for estimating the degree of crystallinity of native cellulose using the X-ray diffractometer, Textil. Res. J. 29 (10) (1959) 786–794.
[26] P. Scherrer, Bestimmung der inneren Struktur und der Größe von Kolloidteilchen mittels Röntgenstrahlen, in: Kolloidchemie Ein Lehrbuch, Springer Berlin Heidelberg, Berlin, Heidelberg, 1912, pp. 387–409.
[27] S.J. Pancake, M.L. Karnovsky, The isolation and characterization of a mucopolysaccharide secreted by the snail, otella lactea, J. Biol. Chem. 246 (1) (1971) 253–262.
[28] W.T. Wulandari, A. Rochliadi, I.M. Arcana, Nanocellulose prepared by acid hydrolysis of isolated cellulose from sugarcane bagasse, IOP Conf. Ser. Mater. Sci. Eng. 107 (2016) 12045.
[29] S. Dej-adisai, T. Pitakbut, W. Chatchai, Alpha-glucosidase inhibitory activity and phytochemical investigation of Borassus flabellifer Linn, Afr. J. Pharm. Pharmacol. 11 (2017) 45–52.
[30] K. Nakashima, J. Sugiyama, N. Satoh, A spectroscopic assessment of cellulose and the molecular mechanisms of cellulose biosynthesis in the ascidian Ciona intestinalis, Mar. Genom. 1 (1) (2008) 9–14.
[31] D. Zhang, et al., A nanocellulose polypyrrole composite based on tunicate cellulose, Int. J. Polym. Sci. 2013 (2013) 175609.
[32] T. Brookman, T. Whittaker, Experimental assessment of the purity of α-cellulose produced by variations of the Brendel method: implications for stable isotope (δ13C, δ18O) dendroclimatology, G-cubed 13 (9) (2012).
[33] B. de Campos Vidal, M.L.S. Mello, Collagen type I amide I band infrared spectroscopy, Micron 42 (3) (2011) 283–289.
[34] A. Buranaprathepratt, T. Yanagi, P. Sawangwong, Seasonal variations in circulation and salinity distributions in the upper Gulf of Thailand: modeling approach, Mer 40 (2002) 147–155.
[35] E. Hirose, H. Yamashiro, Y. Mori, Properties of tunic acid in the ascidian Phallusia nigra (ascidiidae, phlebobranchia), Zool. Sci. 18 (2009) 309–314.
[36] N. Masruchin, et al., Particle size distribution and yield analysis of different charged cellulose nanofibrils obtained by TEMPO-mediated oxidation, IOP Conf. Ser. Earth Environ. Sci. 572 (2020) 12045.
[37] T. Saito, et al., Cellulose nanofibers prepared by TEMPO-mediated oxidation of native cellulose, Biomacromolecules 8 (8) (2007) 2485–2491.
[38] X.M. Dong, J.-F. Revol, D.G. Gray, Effect of microcrystallite preparation conditions on the formation of colloid crystals of cellulose, Cellulose 5 (1) (1998) 19–32.
[39] M.S. Sajab, et al., Telescopic synthesis of cellulose nanofibrils with a stable dispersion of Fe(0) nanoparticles for synergistic removal of 5-fluorouracil, Sci. Rep. 9 (1) (2019) 11703.

[40] Y. Zhao, et al., Tunicate cellulose nanocrystals: preparation, neat films and nanocomposite films with glucomannans, Carbohydr. Polym. 117 (2015) 286–296.
[41] S.Y. Oh, et al., Crystalline structure analysis of cellulose treated with sodium hydroxide and carbon dioxide by means of X-ray diffraction and FTIR spectroscopy, Carbohydr. Res. 340 (15) (2005) 2376–2391.
[42] L. Xing, et al., Cellulose I and II nanocrystals produced by sulfuric acid hydrolysis of Tetra pak cellulose I, Carbohydr. Polym. 192 (2018) 184–192.
[43] M. Roman, W.T. Winter, Effect of sulfate groups from sulfuric acid hydrolysis on the thermal degradation behavior of bacterial cellulose, Biomacromolecules 5 (5) (2004) 1671–1677.